Reactive and Functional Polymers 228 (2026) 106886

Contents lists available at ScienceDirect

Reactive and Functional Polymers

journal homepage: www.elsevier.com/locate/react

Remarkable enhancement of the stability against aging of nanocellulose films by the incorporation of boron compounds

Ricardo Almeida [a], Ana Ramos [b], Verner Håkonsen [c], Jonas Deuermeier [d], Thaddeus Maloney [e], Naceur Belgacem [a,f], José Gamelas [a,*]

[a] Department of Chemical Engineering, CERES, University of Coimbra, Rua Sílvio Lima, Pólo II, 3030-790 Coimbra, Portugal
[b] Fiber Materials and Environmental Technologies (FibEnTech-UBI), University of Beira Interior, R. Marquês D'Ávila e Bolama, 6201-001 Covilhã, Portugal
[c] NTNU NanoLab, Norwegian University of Science and Technology (NTNU), Trondheim 7491, Norway
[d] CENIMAT|i3N, Department of Materials Science, School of Science and Technology, NOVA University Lisbon and CEMOP/UNINOVA, Caparica, Portugal
[e] Department of Bioproducts and Biosystems, Aalto University, P.O. Box 16300, Aalto, Finland
[f] Université Grenoble Alpes, CNRS, Grenoble INP, LGP2, 38000 Grenoble, France

ARTICLE INFO

Keywords:
Accelerated aging
Cellulose degradation
Cellulose nanopapers
Deep eutectic solvent
Sodium borohydride
Sulfation

ABSTRACT

Sulfated cellulose nanofibril (S-CNF) films are promising sustainable materials, yet their properties can deteriorate under moist-heat exposure, limiting their long-term performance. Here, the aging behavior of S-CNF films at 80 °C and 65% relative humidity was investigated and the addition of sodium borohydride ($NaBH_4$) as a chemical stabilization strategy is proposed. Neat S-CNF films underwent rapid acidification and cellulose depolymerization with aging, with pH decreasing from 3.7 to 1.9 and the degree of polymerization (DP) of cellulose dropping from 569 to 80 after only two days of aging. Concomitant changes in crystallinity and morphology were observed, which together culminated in the deterioration of several properties after eight days of aging, including a tensile strength reduction from 123 to 3 MPa and very high color changes ($\Delta E = 39.6$). These poor results were attributed to hydrolysis of sulfate ester groups, which intensified acidification, thus leading to accelerated cellulose chain scission and chromophore generation reactions. In contrast, $NaBH_4$ addition resulted in films with a buffered pH of ca. 9, which suppressed cellulose depolymerization (DP going from 801 to 761 after eight days of aging) and preserved the chemical and microstructural integrity of the films during aging. Consequently, the $NaBH_4$-treated films showed a superior mechanical performance (tensile strength of 39 MPa) and exhibited minimal color changes ($\Delta E = 1.7$) after aging. Overall, $NaBH_4$ addition prior to film formation effectively improves the resistance of S-CNF films against moist-heat aging, extending their applicability for long-term and high-performance applications.

1. Introduction

Cellulose nanofibrils (CNFs) continue to attract considerable interest because they combine exceptional intrinsic properties, including high aspect ratio, high strength and stiffness, tunable surface chemistry, biocompatibility, biodegradability and renewability. Accordingly, CNFs are being explored across diverse application areas, such as food packaging, 3D printing, composite materials, water treatment, drug delivery, electronic devices, among others [1,2]. Structurally, CNFs consist of an entangled network of nanofibrils comprising both amorphous and crystalline domains. Depending on the cellulose source and extraction methods, CNFs typically exhibit diameters between 3 and 50 nm, while their lengths can reach several micrometers [3].

CNFs are commonly produced through intensive mechanical processing (e.g., high-pressure homogenization, microfluidization, grinding, etc.), often preceded by enzymatic or chemical pretreatments, such as 2,2,6,6-tetramethylpiperidine-1-oxyl radical (TEMPO)-mediated oxidation, phosphorylation, cationization, sulfation, and carboxymethylation to reduce energy consumption during fibrillation [4]. Despite their effectiveness, chemical pretreatments may involve expensive reactants, long processing times and environmentally hazardous chemicals that are challenging to recycle and reuse, thereby constraining the industrial scalability of CNF production [5].

In this context, deep eutectic solvents (DESs) have emerged as a

* Corresponding author.
E-mail address: jafgas@eq.uc.pt (J. Gamelas).

https://doi.org/10.1016/j.reactfunctpolym.2026.106886
Received 25 June 2026; Received in revised form 21 July 2026; Accepted 29 July 2026
Available online 29 July 2026

greener and increasingly prominent alternative for CNF production. These solvents are typically composed of hydrogen bond donors (HBDs) and hydrogen bond acceptors (HBAs), forming eutectic mixtures with melting points lower than those of the individual components and of an ideal mixture of the components. They can offer several attractive features, including relatively low-cost constituents, straightforward synthesis, tunability, low toxicity and vapor pressure, as well as recyclability and biodegradability [4,6]. DESs may act not only as swelling agents that facilitate the subsequent mechanical processing for CNF production, but can also, through appropriate selection of the HBDs and HBAs, introduce specific chemical functionalities onto the cellulose structure. A noteworthy example is DES-mediated sulfation, which, after mechanical treatment, can yield CNFs with high values of charge density, degree of fibrillation, viscosity and transparency [7,8].

From the sulfated CNF (S-CNF) dispersions, films/nanopapers with excellent mechanical properties and outstanding optical transparency can be prepared, making them attractive for several applications [9–11]. Nonetheless, for their effective use in long-term applications, nanocellulose films must demonstrate high durability and resistance when exposed to environmental stressors, such as moisture and heat. To the best of our knowledge, the stability of S-CNF films against moist-heat aging has not yet been investigated; however, the limited literature available indicates that the properties of CNF films containing carboxyl or phosphate functionalities can be severely compromised when subjected to moist-heat artificial aging [12–14]. For instance, Camargos et al. [13] reported that TEMPO-oxidized CNF films aged at 80 °C and 75% of relative humidity (RH) for 168 h exhibit notable color changes (darkening and yellowing), a reduction in degree of polymerization (from 198 to 107), and a decrease in crystallinity (75 to 66%) compared to the unaged films. Likewise, highly phosphorylated CNF films (with 2.5 mmol/g of phosphate groups) aged at 80 °C and 65% RH showed pronounced cellulose depolymerization, tensile strength loss and yellowing: 75% loss of their initial degree of polymerization (DP) and 63% of their tensile strength, after eight days of aging, while colorimetric analyses confirmed yellowing, which was also visually evident [12]. Sakiyama et al. [14] further demonstrated, via liquid-state ^{31}P NMR, that moist-heat aging can induce dephosphorylation, resulting in the release and accumulation of free inorganic phosphate salts within phosphorylated CNF films. The accumulation of these salts decreases the pH of the films, thereby accelerating cellulose depolymerization and ultimately contributing to a reduction in fibril length. Collectively, these findings highlight the sensitivity of functionalized CNF films to moist-heat conditions and raise the possibility that S-CNF films may face identical stability challenges, reinforcing the need for the development of chemical stabilization strategies.

Given the limited research on the stability against aging of CNF films and the strong influence that distinct surface functional groups may exert on degradation, it is essential to extend this investigation to other CNF types and to search for mitigation measures in the case of properties' deterioration. In this work, S-CNF films with high sulfation degree were prepared by solvent casting a CNF suspension produced from the pretreatment of a bleached cellulosic pulp with a DES composed of sulfamic acid and urea. The resulting films were then subjected to artificial aging at 80 °C, 65% RH for up to eight days and their degradation was tracked by evaluating their mechanical, optical, chemical, and morphological properties, as well as the degree of cellulose polymerization, pH, crystallinity, and thermal stability. To enhance the moist-heat resistance of the S-CNF films, a novel, straightforward and effective stabilization strategy is proposed based on the incorporation of sodium borohydride ($NaBH_4$) prior to film formation. Accordingly, we hypothesize that $NaBH_4$-treated films will demonstrate superior stability against moist-heat aging compared with the neat S-CNF films.

2. Materials and methods

2.1. Materials

The S-CNF were produced from a bleached *Eucalyptus Globulus* kraft pulp (BEKP), supplied by the Navigator Company, with a composition of 73.0 wt% of cellulose, 18.3 wt% of xylan and 0.8 wt% of soluble lignin (no detectable amount of klason lignin). Urea ($\geq$ 98.5%, pearls, from PanReac AppliChem) and sulfamic acid ($\geq$ 99.5%, from Chem-Lab NV) were the reactants used for the sulfation reaction.

Sodium borohydride ($NaBH_4$, $\geq$ 98.0%) was purchased from Sigma-Aldrich and used without further purification.

2.2. S-CNF production and characterization

The S-CNF was obtained from the sulfation reaction between the BEKP fibers and a DES composed of sulfamic acid and urea, as described by Sirviö et al. [8]. Prior to the reaction, an aqueous suspension of BEKP (consistency of 1.5%) was mechanically stirred overnight, then filtered, washed in ethanol, filtered again and dried in an oven at 60 °C for 24 h. Then, the DES was prepared by mixing 71.9 g of sulfamic acid and 88.9 g of urea (1:2 molar ratio) under magnetic stirring at 80 °C until a clear solution was formed. Subsequently, 20 g of BEKP (dry weight) was added to the DES, and the reaction was carried out at 150 °C for 30 min, with continuous manual stirring using a glass rod. After the reaction, the sulfated pulp was filtered and repeatedly washed with distilled water until the filtrate had a neutral pH. The mass yield of the sulfation reaction, calculated as the mass of the obtained sulfated pulp divided by the theoretical mass expected for a 100% yield, was 72%. The mass of product for 100% yield was estimated considering the mass of the starting pulp (on a dry basis) and the degree of substitution achieved.

After the pretreatment step, the sulfated fibers were diluted with distilled water up to 1 wt% suspension and submitted to two passes in a high-pressure homogenizer (GEA Niro Soavi PandaPlus2000), with the first pass at 500 bar and the second pass at 1000 bar.

The produced S-CNF was characterized according to previously established protocols [9], resulting in a sulfate group content of 2.2 $\pm$ 0.1 mmol/g and a corresponding degree of substitution of 0.47 $\pm$ 0.02. Furthermore, the S-CNF exhibited a degree of polymerization of 823 $\pm$ 2, a degree of fibrillation of ~100%, an optical transmittance of 97.2 $\pm$ 0.2% (for 0.1% suspensions at 600 nm), a zeta potential of -99 ± 3 mV and an average nanofibril diameter of 3.5 $\pm$ 0.4 nm. The nanofibril diameter of S-CNF was determined from atomic force microscopy (AFM) images using Gwyddion software. AFM imaging was performed on the top surface of a S-CNF film (20 g/m^2) prepared by solvent casting using a Bruker Dimension Icon AFM microscope. Two images were acquired at two different locations using a scan area of 1 $\times$ 1 μm^2, a resolution of 512 data points per line and a scan rate of 0.5 Hz. The diameters were measured from the AFM images as the widths of the fibrils. The reported average nanofibril diameter was determined from a total of 80 width measurements performed using the Gwyddion software, with 40 measurements for each AFM image. In each image, half of the measurements (20) were randomly taken from the upper part and the remaining 20 from the lower part, ensuring that the measurements were representative of the entire AFM image area. The corresponding AFM images of S-CNF are shown in Fig. 1.

2.3. Preparation of S-CNF films

The S-CNF films were prepared by solvent casting 0.2 wt% aqueous S-CNF suspensions, previously stirred at 1000 rpm for 10 min using a high-shear disperser (Dispermat CV3-PLUS-E). The suspensions were poured into 9 cm-diameter polystyrene Petri dishes and left drying at room temperature for 7 days in a fume hood. After drying, the films were detached and stored prior to artificial accelerated aging. All films were designed to have a basis weight of approximately 20 g/m^2.

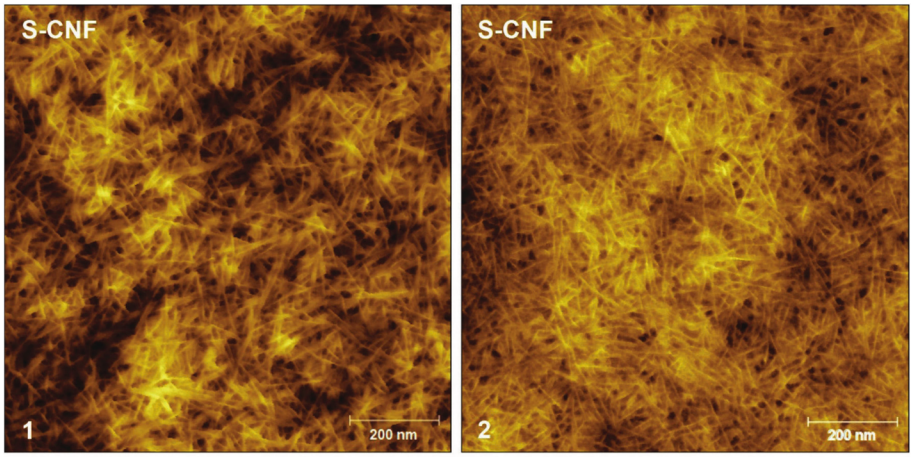

Fig. 1. AFM images of S-CNF used to determine the nanofibril diameters.

To enhance the resistance of S-CNF films to artificial moist-heat aging, an optimized amount of $NaBH_4$ (0.1 g $NaBH_4$ per g of dry S-CNF) was added to the 0.2 wt% S-CNF suspension, followed by overnight stirring at room temperature. Next day, the suspensions were stirred again in the high-shear disperser and cast into Petri dishes to dry under the same conditions described above for the neat S-CNF films. The $NaBH_4$ dosage was selected based on preliminary optimization experiments, in which the optical and mechanical properties of S-CNF films prepared with varying amounts of $NaBH_4$ were evaluated before and after 8 days of aging. The chosen dosage (0.1 g $NaBH_4$ per g of dry S-CNF) corresponded to the amount that minimized variations in these properties between aged and unaged films.

Hereafter, the $NaBH_4$-treated films are designated as S-CNF_{NaBH4} to differentiate them from the neat S-CNF films.

2.4. Artificial accelerated aging of the S-CNF and S-CNF_{NaBH4} films

The prepared S-CNF and S-CNF_{NaBH4} films were subjected to the same accelerated moist-heat aging protocol in a Memmert Humidity chamber (HCP108) at 80 °C and 65% RH, based on ISO 5630-3:1996. The films were aged for up to 8 days, during which the S-CNF films were removed from the chamber every two days, while the S-CNF_{NaBH4} films were collected only after four and eight days of exposure. All film samples were subsequently stored for further characterization.

2.5. Characterization of the unaged and aged S-CNF and S-CNF_{NaBH4} films

All films were characterized in terms of the DP of cellulose, pH, crystallinity, mechanical and optical properties, morphology, chemical structure and thermal stability.

The DP was estimated from intrinsic viscosity (η) measurements in cupriethylenediamine, based on ISO 5351:2010. The films were first cut into small square pieces and oven-dried at 50 °C for 24 h. The film fragments were then mixed with 25 mL of distilled water with glass spheres under magnetic stirring (at 700 rpm for 30 min). Subsequently, 25 mL of a 0.5 M cupriethylenediamine solution was added and the mixture was stirred using a mechanical rotary stirrer for 30 min. Intrinsic viscosity measurements were performed at 25 °C using a standard capillary viscometer. The corresponding DP values were calculated using the Mark-Houwink equation ($\eta = k \times DP^a$), with the following parameters: $k = 0.42$ and $a = 1$ (for DP < 950); $k = 2.28$ and $a = 0.76$ (for DP > 950) [15].

Before pH measurements, the films were also cut into small square pieces and dried in an oven at 50 °C for 24 h. Subsequently, 0.1 g of the dried film was dispersed in 10 mL of deionized water under magnetic stirring for 1 h at room temperature. The pH of the resulting dispersion was measured using a calibrated pH meter (Hanna Instruments pH meter HI2210).

The crystallinity of the prepared films was evaluated by X-ray diffraction using a Bruker D8 ADVANCE diffractometer operating in the Bragg-Brentano geometry with Cu-Kα ($\lambda = 1.54$ Å) source at a current of 40 mA and an accelerating voltage of 40 kV. The data were collected by the step counting method (step size: 0.01° and counting time: 0.5 s) over a 2θ range of 5–60°. The crystallinity index values were determined using the empirical Segal method [16].

The mechanical properties (tensile strength, Young's modulus and elongation at break) were determined according to ISO 1924-2 using a Thwing-Albert Instrument Co tensile tester. The tensile tests were conducted at 23 ± 1 °C and 50 ± 2% RH, with a strain rate of 10 mm/min and an initial distance between grips of 50 mm. Reported values correspond to the average of four specimens for two replicate films. The basis weight and thickness of the films were also determined under the same pre-conditioning conditions before tensile testing. Basis weight was calculated as the ratio between the film mass and its area, while thickness was measured using an Adamel Lhomargy MI 20 micrometer and reported as the average of five measurements taken at different points of each film.

The optical properties evaluated in the films were transparency, CIE L*a*b* color coordinates and specular gloss. The transparency was measured according to the ISO 22891, using a Technidyne Color Touch 2 spectrophotometer; measurements on two replicate films were made applying the illuminant D65 and a 10° standard observer at the wavelength of 557 nm. The colorimetric measurements were performed using the same spectrophotometer, also operating in D65/10° mode. The results are expressed in the CIE L*a*b* color space, where "L" coordinate refers to lightness, ranging from black (0) to white (100), "a" indicates the color shift between green (−) and red (+), and "b" represents the variation between blue (−) and yellow (+). The color difference (ΔE) between the unaged and aged films was then calculated based on the color coordinates as follows:

$$\Delta E = \sqrt{(\Delta L^*)^2 + (\Delta a^*)^2 + (\Delta b^*)^2}$$

The specular gloss of the films was evaluated according to the ISO 2813 standard using a Hach Lange REFO 3D Glossmeter, at an angle of incidence of 60° over an area of 17 mm × 9 mm. Measurements were taken on two replicate films, each measured in duplicate, and all results are reported in gloss units (GU) with respect to a polished black glass standard.

The cross-sectional morphology of the films was analyzed by field emission scanning electron microscopy (FE-SEM). The SEM micrographs

(captured at magnification of 4000× and 8000×) were acquired using a Thermo Fisher Scientific Apreo scanning electron microscope, with the in-lens secondary electron detector; an acceleration voltage of 2 kV and a beam current of 13 pA were applied. Prior to imaging, the films were submerged in liquid nitrogen and fractured to expose the cross-sections. No conductive coating was applied to the samples for charge dissipation.

The chemical features of the films were assessed by Fourier transform infrared (FTIR) spectroscopy in the attenuated total reflection (ATR) mode and X-ray photoelectron spectroscopy (XPS). The FTIR spectra were recorded using a JASCO FT/IR-4X spectrometer, in the range of 350–4000 cm^{-1}, with a resolution of 4 cm^{-1} and 128 scans. XPS was performed using a Kratos AXIS Supra spectrometer equipped with a monochromatic Al Kα X-Ray source operating at 150 W. The wide-scan survey spectra were acquired using a pass energy of 80 eV, while high-resolution spectra were recorded with a pass energy of 10 eV. A low energy electron flood gun was used for charge neutralization, with C 1 s adjusted to 285 eV a posteriori. Data analysis was carried out using CasaXPS software, version 2.3.25PR1.0.

The thermal analysis of the films was performed using a SDT Q600 thermal analyzer (TA instruments). The film samples were heated from room temperature up to 1000 °C, at a rate of 10 °C/min, under a nitrogen flow of 100 mL/min. From the obtained thermograms and the corresponding derivative curves, the onset degradation temperature (T_{on}), the temperature(s) of maximum degradation rate (T_{max}) and the char residue were determined, as previously described [9].

3. Results and discussion

3.1. Effect of moist-heat aging on the DP, pH and crystallinity of S-CNF and S-CNF_{NaBH4} films

It is well known that the aging of cellulose materials (e.g., paper) is typically characterized by a decrease in the cellulose DP, which occurs as a consequence of cellulose degradation via acid-catalyzed hydrolysis and/or oxidation [17]. In this context, the degradation of S-CNF and S-CNF_{NaBH4} films was tracked by measuring their DP (Fig. 2a) and pH (Fig. 2b) at different aging times.

From the DP values estimated from the intrinsic viscosity measurements, it was found that the cellulose DP of the unaged S-CNF film (DP = 569) was about 30% lower than that of the starting S-CNF suspension (DP = 823). Because the film was solvent cast at room temperature, comparable DP values would be expected; however, this was not observed. This indicates that cellulose depolymerization occurred during casting/drying stage, which is in line with the pronounced acidification effect observed after film formation, as the pH value of the unaged S-CNF film (3.7) was substantially lower than that of the initial 0.2 wt% S-CNF suspension (pH = 6.9). This pH decrease may have been partially driven by the presence of free acidic sulfate species, such as HSO_4^-. Such acidification favored acid-catalyzed hydrolytic cleavage of β-1,4-glycosidic bonds, explaining the lower cellulose DP obtained for the unaged S-CNF film. In contrast, when $NaBH_4$ was incorporated prior to film formation, the cellulose DP of the unaged S-CNF_{NaBH4} film remained close to that of starting S-CNF suspension (801 and 823, respectively). In this case, the pH of the 0.2 wt% S-CNF suspension after $NaBH_4$ addition (pH = 9.1) and that of the corresponding S-CNF_{NaBH4} film (pH = 8.9) were very similar, indicating that the pH of the medium remained alkaline during casting, thereby minimizing cellulose depolymerization.

After aging the neat S-CNF films at 80 °C and 65% RH, a sharp decline in cellulose DP was observed after only two days, decreasing from 569 to 80, after which the DP values remained approximately constant throughout the subsequent aging period (Fig. 2a). This trend is consistent with the measured pH values of the S-CNF films, which also exhibited a marked decrease from 3.7 in the unaged film to 1.9 after two days of aging (Fig. 2b), with similar pH values recorded thereafter. The high acidity of the S-CNF films, combined with the moist-heat aging conditions, promoted an extensive cleavage of cellulose glycosidic bonds, ultimately resulting in the drastic DP reduction just after two-days aging. Cellulose depolymerization of CNF films bearing other chemical functional groups (e.g., carboxyl and phosphate groups) has also been reported under comparable aging conditions. For instance, Camargos et al. [13] reported that a TEMPO CNF film (1.6 mmol/g of carboxyl groups) exhibited a 46% reduction in DP compared with the unaged film after seven days of aging at 80 °C and 75% RH. More recently, Almeida et al. [12] also showed that highly phosphorylated CNF films with a phosphate content of ca. 2.5 mmol/g undergo pronounced cellulose depolymerization, with a DP reduction of 75% after eight days of aging at 80 °C and 65% RH. Considering that the S-CNF films prepared in the present study lost 86% of their initial DP in just two days of aging and 87% after eight days, these results suggest that sulfate groups introduced into the cellulose backbone may promote faster and more severe acid-catalyzed cellulose depolymerization under moist-heat conditions than comparable contents of carboxyl or phosphate functionalities.

Given the substantial decrease in cellulose DP observed for the neat S-CNF films during aging, which can adversely affect key functional properties, namely mechanical performance, $NaBH_4$ was incorporated (0.1 g per g of dry S-CNF) to mitigate cellulose depolymerization. As

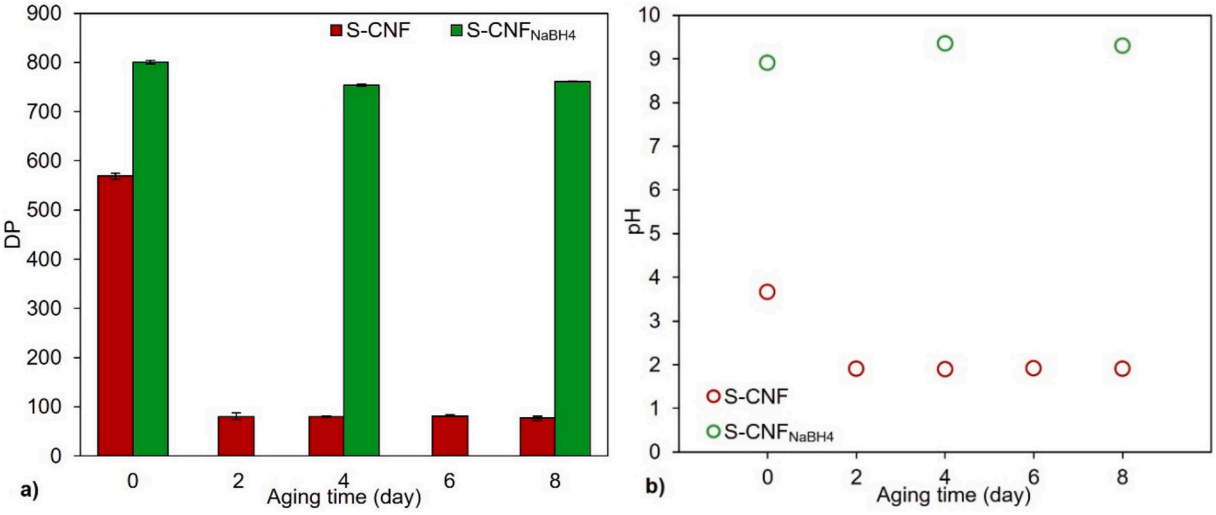

Fig. 2. DP (a) and pH (b) as function of aging time for the S-CNF and S-CNF_{NaBH4} films.

showed in Fig. 2a, this strategy proved highly effective, with the S-CNF$_{NaBH4}$ films losing only 5% of the initial cellulose DP after eight days of aging (decreasing from 801 to 761), whereas the neat S-CNF films exhibited a pronounced loss of 87% over the same period. The strong stabilizing effect of the addition of $NaBH_4$ on cellulose DP of the S-CNF$_{NaBH4}$ films can be attributed both to the increase in pH after $NaBH_4$ addition and to the buffering effect imparted by the treatment. Upon incorporation of $NaBH_4$ into the 0.2 wt% S-CNF suspension, the pH of the suspension increased from 6.9 to 9.1, which was also reflected in the resulting films: the unaged S-CNF$_{NaBH4}$ film exhibited a pH of 8.9, while the corresponding neat S-CNF film showed a pH of 3.7 (Fig. 2b). The increase in pH observed in both suspensions and films can be explained by the self-hydrolysis of $NaBH_4$ in aqueous medium, which occurs under acidic, neutral and even moderately alkaline conditions. $NaBH_4$ is chemically stable only under strongly alkaline conditions, with a half-life time of approximately 42 days at pH 13 [18]. Therefore, because the initial pH of the S-CNF suspension was near neutral, $NaBH_4$ must have undergone very fast hydrolysis immediately after its addition to the suspension, forming sodium borate products and hydrogen gas, according to the following global reaction: $NaBH_{4(s)} + 4H_2O_{(l)} \rightarrow NaB(OH)_{4(aq)} + 4H_{2(g)}$ [19]. In fact, considering that the half-life time of $NaBH_4$ at pH 7 is ca. 3.7 s (calculated from the empirical formula reported by Retnamma et al. [19]) and assuming that $NaBH_4$ hydrolysis follows a first-order kinetics [20], 99% conversion of $NaBH_4$ into borates may require only 24.4 s. As the resulting boron species confer alkaline pH, the pH of the suspensions and corresponding films increased. Besides the higher pH value of the unaged S-CNF$_{NaBH4}$ film, Fig. 2b also shows that after four and eight days of aging the pH remained reasonably similar to that of the unaged homologue, a behavior not observed for the S-CNF films. This trend is explained by the formation of the $B(OH)_4^-/B(OH)_3$ conjugated pair during $NaBH_4$ hydrolysis, which is known to act as a buffer in the pH range of approximately 8–10 [21]. As no washing step was performed after $NaBH_4$ incorporation, the boron by-products formed remained entrapped within the films after drying, thereby preserving the buffering effect during aging. This buffering capacity enables the S-CNF$_{NaBH4}$ films to neutralize acidic species that may be formed during aging, limiting pH fluctuations. Overall, because the $NaBH_4$ treatment increased and stabilized the film pH around 9, the hydrolytic degradation of the S-CNF$_{NaBH4}$ films was largely suppressed, as evidenced by the very similar DP values obtained for the unaged and aged films (DP loss of only 5%). It is also well known that $NaBH_4$ can selectively convert carbonyl groups (e.g., aldehydes and ketones) into hydroxyl groups, which may also contribute to an improvement in DP retention and color stability during aging [22]. However, considering the very high self-hydrolysis rate of $NaBH_4$ under the conditions of film preparation used in this study (initial pH of ca. 7), it is unlikely that any unreacted $NaBH_4$ remained available in the film, after the film preparation, to act as a reducing agent during the aging of the S-CNF$_{NaBH4}$ films. Furthermore, neither FTIR analysis nor XPS analysis (shown below) provided evidence that carbonyl group reduction had occurred. $NaBH_4$ may have acted as reducing agent only in the early instants after its addition to the S-CNF suspension (during the film preparation) and not during the aging of the films where it is no longer present.

Since the films were prepared by solvent casting, the boron content retained in the final S-CNF$_{NaBH4}$ films is expected to be equivalent to the amount of $NaBH_4$ initially added to the S-CNF suspension (i.e., 0.1 g $NaBH_4$/g of dry S-CNF). Accordingly, the maximum content of boron in the $NaBH_4$-treated films is calculated to be 0.029 g per g of dry S-CNF (2.9%, w/w). Thus, the presence of ca. 3% of boron in these films may limit their use in certain regulated applications, such as food packaging, cosmetics and biomedical materials. However, for other applications, such as electronic devices or the conservation and restoration of historical objects, the presence of boron-containing species may be less problematic. Nevertheless, to identify the most suitable applications for the S-CNF$_{NaBH4}$ films, leaching tests, toxicity studies and exposure assessments should be addressed in the future. A comparative life-cycle assessment of both the neat and $NaBH_4$-treated films would also be useful to determine whether boron incorporation imposes an additional environmental burden. Nonetheless, exposure of adult humans to boric acid and borates has been reported to be reasonably safe when exposure levels are low [21]. Even in cases of relatively high exposure, such as in regions where drinking water contains high concentrations of boron compounds or among workers in mining and industrial environments, toxicity in humans is reportedly uncommon [23]. However, exposure to boron species requires particular attention in sensitive populations, including neonates, young children and pregnant woman [21].

The crystallinity of S-CNF and S-CNF$_{NaBH4}$ films before and after four and eight days of aging was also assessed by X-ray diffraction, with the resulting diffractograms and crystallinity index (CrI) values shown in Fig. 3.

As shown in Fig. 3a, the unaged neat S-CNF film displayed two characteristic diffraction peaks at $2\theta = 14.9^\circ$ and 22.1° assigned to the $(1\bar{1}0 + 110)$ and (200) lattice planes of cellulose I polymorph [24]. Compared with other CNF films containing carboxyl [13] and phosphate groups [12], the unaged S-CNF film exhibited a relatively low crystallinity index (CrI) of 42.5%, which could contribute to a lower stability against aging, as lower cellulose crystallinity is often associated with higher accessibility to water and enhanced susceptibility to degradation [25].

The two diffraction peaks observed in the unaged S-CNF film were also detected in the corresponding films aged for four and eight days at nearly identical Bragg angles, indicating that the native cellulose I structure was preserved even after artificial moist-heat aging. Nevertheless, the peaks in the aged S-CNF films were more intense than in the unaged film, resulting in higher CrI values: increase from 42.5% (unaged) to 61.8% and 65.7% after four and eight days of aging, respectively. Such increases in crystallinity after moist and heat exposure have been reported for other cellulosic materials, including cellulose paper [26] and bacterial cellulose films [27]. This behavior may be attributed to preferential degradation of the amorphous regions of cellulose during moist-heat aging, possibly accompanied by the rearrangement or reorientation of cellulose chains within these regions, promoting recrystallization [28,29].

In contrast to the S-CNF films, more similar diffractograms and CrI values were obtained for the $NaBH_4$-treated films before and after aging (Fig. 3b). After eight days aging, the CrI of the aged S-CNF$_{NaBH4}$ film was only 4.4% higher (absolute increase) than that of the unaged film, whereas for the neat S-CNF films a substantially larger increase (23.2%) was found. Because the S-CNF$_{NaBH4}$ films experienced minimal cellulose depolymerization during aging due to the $NaBH_4$ treatment, the apparent increase in crystallinity, commonly associated with degradation of the amorphous domains, was far less pronounced than that in the neat S-CNF films.

3.2. *Effect of moist-heat aging on the mechanical properties of the S-CNF and S-CNF$_{NaBH4}$ films*

The mechanical performance of the S-CNF and S-CNF$_{NaBH4}$ films before and after aging was evaluated in terms of tensile strength (T.S), Young's modulus (E) and elongation at break (E.B), with the results shown in Fig. 4.

As expected from the significant cellulose depolymerization and crystallinity changes observed for the neat S-CNF films with aging, their mechanical properties also markedly deteriorated. Similarly to the cellulose DP evolution, the most substantial losses occurred within the first two days of aging. For example, the T.S decreased from 123 MPa in the unaged film to only 5 MPa. In the subsequent days, the T.S values remained very low and relatively constant, and this trend was also observed for the E and E.B. In other words, just two days of aging at 80 °C and 65% RH caused the S-CNF films to lose nearly all mechanical integrity, with reductions of 96%, 79% and 87% in T.S, E and E.B,

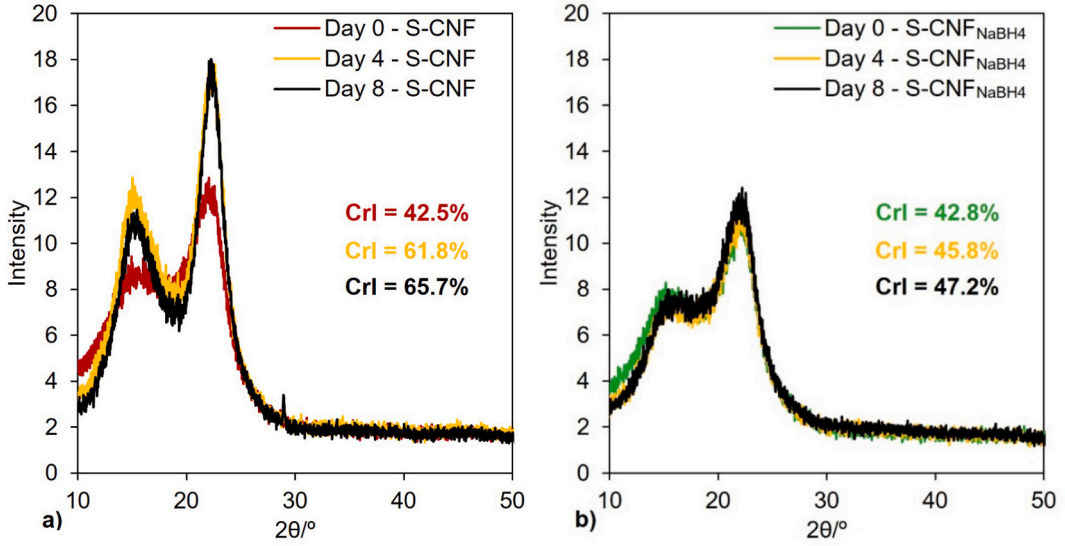

Fig. 3. X-ray diffractograms and corresponding crystallinity index values for the S-CNF films (a) and S-CNF$_{NaBH4}$ films (b) before aging and after four and eight days of aging.

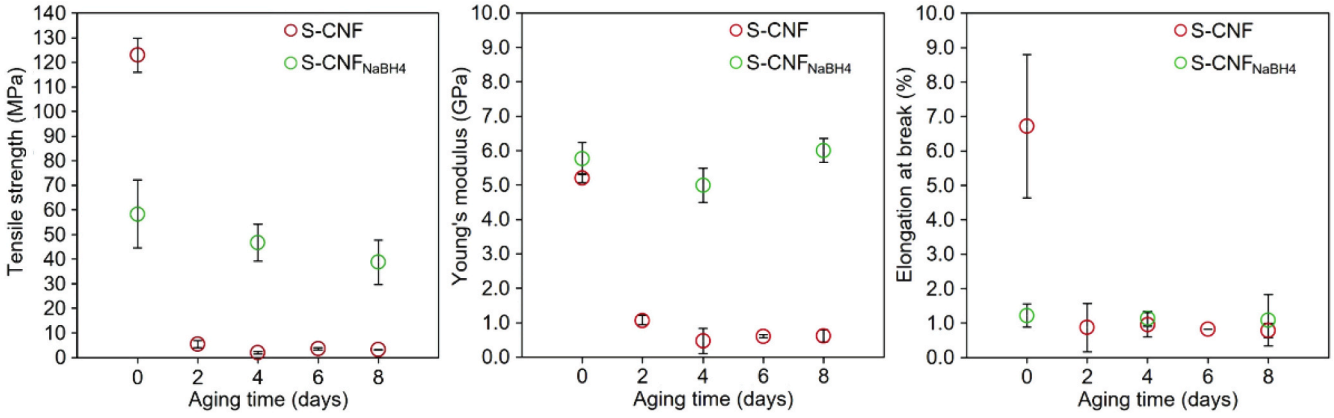

Fig. 4. Mechanical properties of the S-CNF and S-CNF$_{NaBH4}$ films as function of aging time.

respectively. The mechanical deterioration of the S-CNF films was considerably higher than that reported by Almeida et al. [12] for highly phosphorylated CNF films (2.5 mmol/g of phosphate groups) aged for the same time under the same conditions of temperature and relative humidity, the latter showing losses of only 38%, 31% and 16% in the T.S, E and E.B, respectively. This highlights, once again, the critical role of surface chemistry in the stability against aging of CNF-based materials. Besides cellulose depolymerization and crystallinity changes, additional factors may have contributed to this severe mechanical deterioration of the films during aging, including weakening of the hydrogen-bonding network between the nanofibrils and variations in film apparent density. Indeed, a sharp decrease in apparent density was observed for the films after aging due to increased film thickness: the unaged S-CNF film exhibited an apparent density of 1.32 g/cm^3, while the eight-days aged film showed a density value of only 0.75 g/cm^3. This reduction likely further contributed to the lower tensile performance of the aged S-CNF films, as higher apparent density typically favors the mechanical properties of CNF films [30].

For the S-CNF$_{NaBH4}$ films, such pronounced deterioration of the mechanical properties during moist-heat aging was not observed. Notwithstanding, before aging, Fig. 4 shows that they presented lower T.S (58 MPa) and E.B (1.2%) compared with the neat S-CNF films (123 MPa and 6.7%, respectively). Because no rinsing step was performed after $NaBH_4$ treatment, the borate species retained within the films likely reduced the number of fibril-fibril interactions and hindered the physical entanglement of the fibrils, resulting in a lower mechanical strength of the S-CNF$_{NaBH4}$ film before aging. Despite this initial decrease, the S-CNF$_{NaBH4}$ films exhibited considerably higher mechanical stability during aging. While the T.S and E of the neat S-CNF films decreased dramatically from 123 MPa and 5.2 GPa to only 2 MPa and 0.5 GPa after four-days aging, for the S-CNF$_{NaBH4}$ films only slight and not statistically significant decreases from 58 MPa and 5.8 GPa to 47 MPa and 5.0 GPa were observed. Even after eight-days aging, the $NaBH_4$-treated film lost only ca. 34% of its initial T.S, whereas the neat S-CNF film lost about 97%.

Because $NaBH_4$ treatment resulted in films showing minimal variations in cellulose DP (801–761), crystallinity index (43–47%) and apparent density (1.4–1.5 g/cm^3) during aging, the S-CNF$_{NaBH4}$ films were able to retain superior mechanical properties compared with the S-CNF films.

3.3. *Effect of moist-heat aging on the optical properties of the S-CNF and S-CNF$_{NaBH4}$ films*

The optical properties of cellulose-based materials are also typically compromised during aging due to the formation of chromophores,

resulting in the characteristic yellowing of those materials [25]. Accordingly, the optical stability of the S-CNF and S-CNF_{NaBH4} films was evaluated by measuring their CIE L*a*b* coordinates, optical transparency and specular gloss (Table 1). Digital photographs of both film types before and after aging are presented in Fig. 5.

As indicated in Table 1, the CIE L*a*b* coordinates changed significantly with aging, resulting in pronounced color differences (ΔE) between the unaged and aged S-CNF films. The aged S-CNF films consistently exhibited lower values in L* coordinate (lightness) and higher values in a* (green to red) and b* (blue to yellow) coordinates compared with those obtained for the unaged S-CNF film, indicating a progressive shift toward darker, redder and more yellow tones. These changes were visually perceptible as darkening and yellowing, giving the films a brownish appearance, particularly after eight days of aging (Fig. 5). The ΔE values progressively increased with aging time, having been reached considerably high ΔE values (12.7–39.6) from the fourth day onward. According to the criteria defined by Mokrzycki and Tatol [31], whereby a standard observer can notice two distinct colors when $\Delta E > 5$, only the S-CNF film aged for two days ($\Delta E = 3.5$) remained below this threshold. Similar to what happened with cellulose DP and mechanical properties, the color differences between the unaged and aged S-CNF films, particularly after eight days of aging ($\Delta E = 39.6$), were considerably higher than those reported by Almeida et al. [12] and Camargos et al. [13] for phosphorylated CNF and TEMPO CNF films subjected to moist-heat aging.

In the present work, the addition of an appropriate amount of $NaBH_4$ was explored as a strategy to mitigate yellowing of the films under moist-heat aging. When $NaBH_4$ was incorporated, the CIE L*a*b* coordinates of the corresponding aged films (S-CNF_{NaBH4}) were very similar to those of the unaged film. In fact, after eight days of aging, the L* and a* coordinates remained nearly unchanged, while the b* coordinate increased very slightly from −6.9 to −5.2, but still maintaining the value in the blue zone. Owing to these small variations in the color coordinates, the resulting color differences (ΔE) between the unaged and aged S-CNF_{NaBH4} films were markedly lower compared to those obtained for the S-CNF films: ΔE values did not exceed 1.7 for the S-CNF_{NaBH4} films, whereas for the S-CNF films after four- and eight-days aging, ΔE values of 12.7 and 39.6, respectively, were obtained. Typically, with ΔE values below 2.0, color differences between two samples are not perceptible by a standard observer [31], which is in agreement with the digital photographs of the S-CNF_{NaBH4} films shown in Fig. 5.

Overall, the $NaBH_4$ treatment imparted great color stability to the S-CNF_{NaBH4} films which was not observed for the neat S-CNF films, suggesting that $NaBH_4$ was able to limit the formation of chromophore structures, such as carbonyl-containing functionalities and alkenes. Although $NaBH_4$ is known to be a reducing agent able to selectively convert carbonyl groups into hydroxyl groups [32], it is unlikely that this occurs in the present case due to its fast self-hydrolysis under the pH conditions of film preparation, as described above. The color stabilization of the films (with aging) could be related to the buffering effect of the formed borates/boric acid, limiting not only the acid-catalyzed cleavage (hydrolysis) of cellulosic glycosidic bonds but also acid-catalyzed dehydration processes (e.g., pinacol rearrangement on the C2,C3 diol of cellulose or alkene formation at C5-C6 position), responsible for chromophore generation. Note that cellulose hydrolysis itself also introduces carbonyl groups through the formation of new reducing ends containing aldehyde groups at the C1 position, thus acting as a precursor reaction for chromophores.

Owing to the high fraction of nanosized fibrils (degree of fibrillation of ca. 100%) and their very small dimensions, all films (unaged and aged) exhibited very high transparency values, ranging from 93.4% to 94.8%. Interestingly, the presence of residual borate species in the S-CNF_{NaBH4} films, resulting from the $NaBH_4$ treatment, did not negatively affect film transparency, as evidenced by the same transparency values obtained for the unaged S-CNF and S-CNF_{NaBH4} films (94.7%). After aging at 80 °C and 65% RH, the transparency showed no variation for the S-CNF_{NaBH4} films, whereas for the neat S-CNF films only a very small decrease (≤1%) could be noted compared to the unaged film. These results are in line with those reported by Almeida et al. [12] for phosphorylated CNF films, indicating that the optical transparency of CNF films is not significantly compromised by moist-heat aging, regardless of their surface chemistry.

Similarly to transparency, the gloss values obtained for the unaged S-CNF (50.5 GU) and S-CNF_{NaBH4} (50.4 GU) films were nearly identical, further indicating that residual borate species did not compromise this property. Gloss is strongly dependent on surface roughness, with higher values typically associated with smoother surfaces [33]. Accordingly, the progressive decrease in gloss values with aging time (Table 1), suggests that the surface topography of both film types was altered during aging, with their surfaces becoming rougher and wrinkled. After eight days, the gloss of the S-CNF and S-CNF_{NaBH4} films decreased from 50.5 to 22.0 GU and from 50.4 to 17.3 GU, respectively, indicating that $NaBH_4$ treatment could not mitigate the gloss loss during aging.

3.4. *Effect of moist-heat aging on the morphological properties of the S-CNF and S-CNF_{NaBH4} films*

The cross-sectional morphology of the S-CNF and S-CNF_{NaBH4} films before and after eight days of aging was examined by SEM, and the resulting micrographs are presented in Fig. 6.

The SEM images shown in Fig. 6 further highlight the differences between the neat S-CNF films and the $NaBH_4$-treated films (S-CNF_{NaBH4}). Before aging, the neat S-CNF film exhibited a well-organized and oriented layered structure with some visible gaps between layers. In contrast, although the S-CNF_{NaBH4} film also displayed a multilayered structure, the layers seem to be less oriented and aligned than those observed in the cross-section of the neat S-CNF film. Furthermore, no evident interlayer gaps were detected in the unaged S-CNF_{NaBH4} film.

SEM micrographs also revealed that the cross-section of the neat S-CNF films underwent significant structural changes during aging, whereas no significant modifications were observed for the S-CNF_{NaBH4} films. Specifically, the aging process led to the collapse of the multilayer structure observed in the unaged S-CNF film, with the individual layers apparently coalescing into a single compact layer. On the other hand, the similar cross-sections exhibited by the unaged and aged S-CNF_{NaBH4} films suggest that $NaBH_4$ treatment also helped to protect the films

Table 1
CIE L*a*b* coordinates, color difference (ΔE), optical transparency and specular gloss of the S-CNF and S-CNF_{NaBH4} films as function of aging time.

		L*	a*	b*	ΔE	Transparency (%)	Gloss (GU)
Day 0	S-CNF	93.3 ± 0.2	1.8 ± 0.1	−6.9 ± 0.2	–	94.7 ± 0.7	50.5 ± 4.6
	S-CNF_{NaBH4}	93.3 ± 0.1	1.7 ± 0.0	−6.9 ± 0.0	–	94.7 ± 0.5	50.4 ± 4.7
Day 2	S-CNF	92.0 ± 0.7	1.8 ± 0.0	−3.7 ± 0.1	3.5	94.8 ± 0.3	50.1 ± 2.6
Day 4	S-CNF	87.2 ± 0.0	2.3 ± 0.0	4.2 ± 0.1	12.7	93.4 ± 1.0	41.7 ± 3.2
	S-CNF_{NaBH4}	93.1 ± 0.1	1.6 ± 0.0	−5.6 ± 0.2	1.3	94.6 ± 0.4	26.5 ± 6.3
Day 6	S-CNF	79.6 ± 0.8	4.2 ± 0.3	15.7 ± 1.4	26.7	94.2 ± 0.3	29.4 ± 7.6
Day 8	S-CNF	71.3 ± 0.5	7.2 ± 0.2	25.6 ± 0.5	39.6	93.6 ± 0.0	22.0 ± 6.3
	S-CNF_{NaBH4}	93.2 ± 0.2	1.6 ± 0.0	−5.2 ± 0.1	1.7	94.7 ± 0.4	17.3 ± 4.1

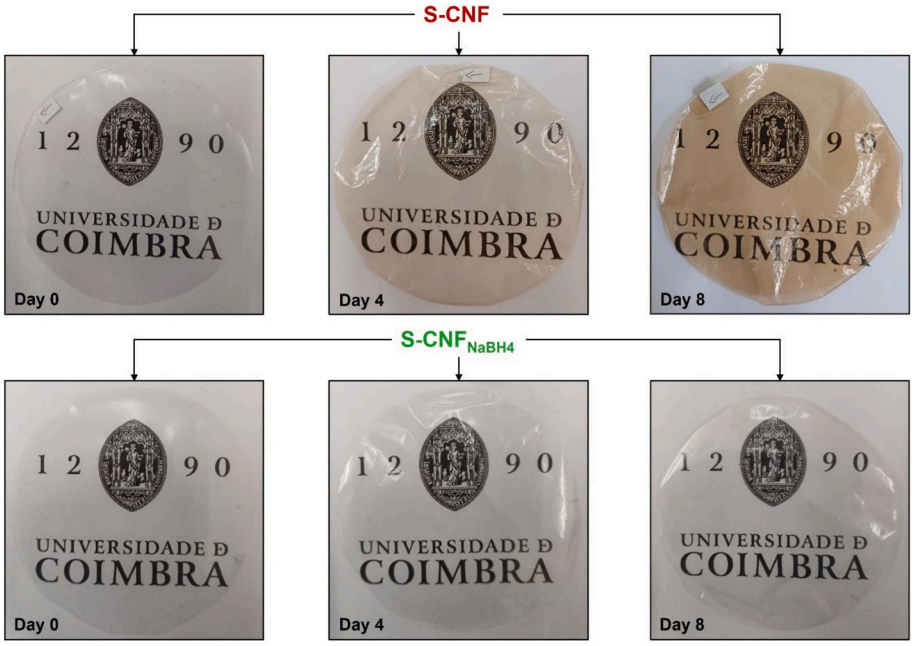

Fig. 5. Digital photographs of the S-CNF and S-CNF$_{NaBH4}$ films before aging and after four and eight days of aging.

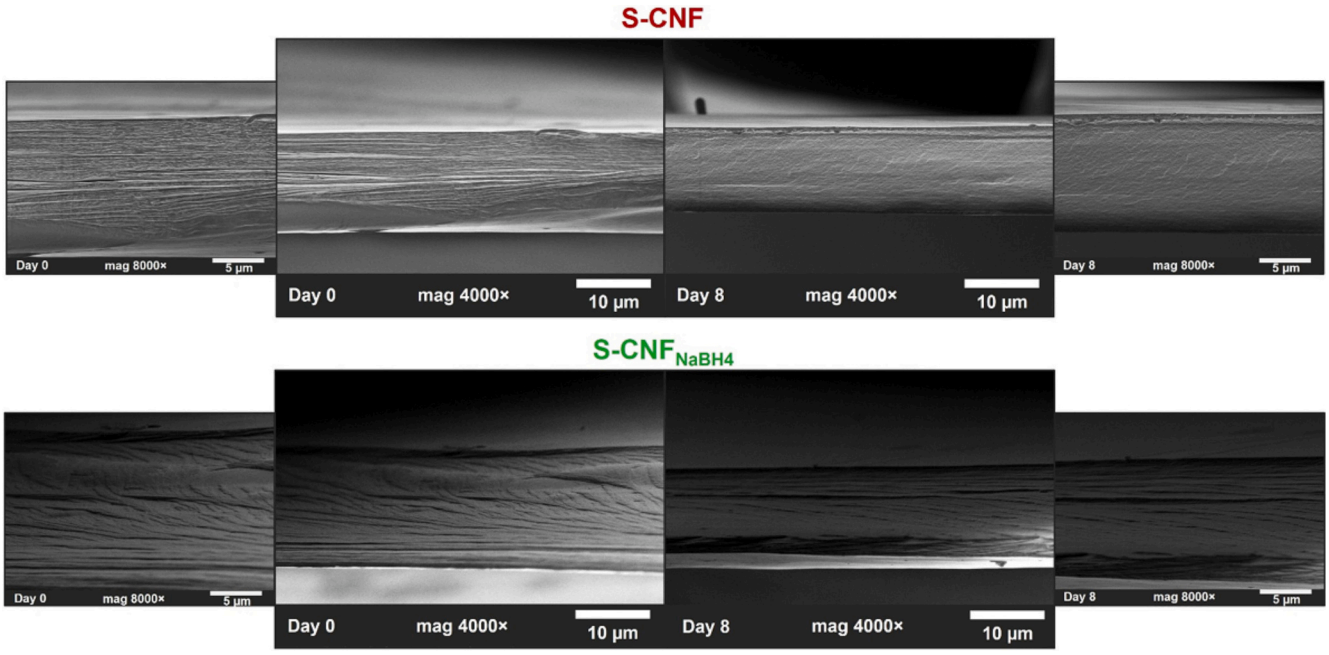

Fig. 6. FE-SEM images (captured at magnification of 4000× and 8000×) of the cross-section of the unaged and aged S-CNF and S-CNF$_{NaBH4}$ films.

against morphological changes during aging. This structural preservation likely contributed to the smaller variations observed in the mechanical properties between the unaged and aged $NaBH_4$-treated films compared with the untreated S-CNF films.

3.5. *Effect of moist-heat aging on the chemical structure of the S-CNF and S-CNF$_{NaBH4}$ films*

The chemical structure of the S-CNF and S-CNF$_{NaBH4}$ films before and after eight days of aging was evaluated using FTIR (Fig. 7) and XPS (Fig. 8).

The incorporation of sulfate functional groups into the cellulose backbone was confirmed by FTIR spectroscopy through the presence of characteristic peaks in the unaged films at 1221–1209 cm^{-1} and 808–805 cm^{-1} corresponding to the asymmetric O=S=O and symmetric C–O–S stretching vibrations, respectively (Fig. 7). An additional absorption peak at 1430 cm^{-1} was also observed in the spectrum of the unaged S-CNF film, which is attributed to the deformation vibration of NH_4^+ due to the presence of ammonium salt of sulfate ester [7,8,11]. However, upon $NaBH_4$ addition, this peak (at 1430 cm^{-1}) was no longer observed. Given that $NaBH_4$ incorporation increased the pH of the 0.2 wt% S-CNF suspension to 9.1 (as discussed above) and considering that alkaline conditions favor deprotonation of NH_4^+ with concomitant ammonia volatilization, the absence of this peak in the S-CNF$_{NaBH4}$ film is likely attributable to NH_4^+ loss under relatively high pH conditions [34]. This assumption was indeed confirmed by XPS analysis as will be

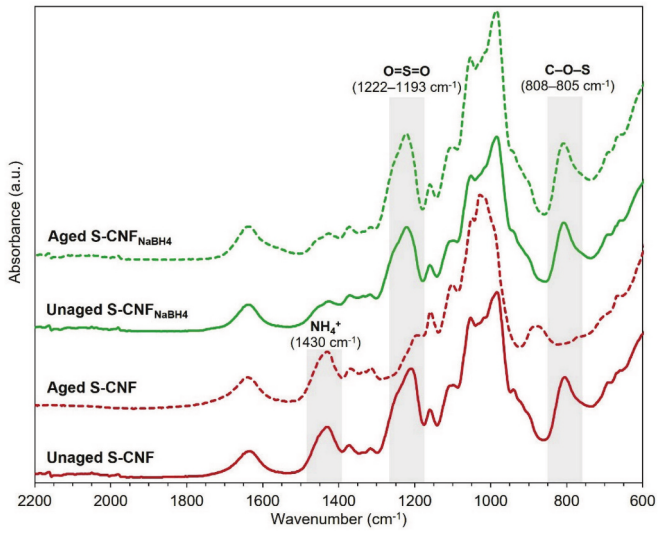

Fig. 7. FTIR spectra of the S-CNF and S-CNF$_{NaBH4}$ films before aging and after eight days of aging.

shown below.

After eight days of moist-heat aging, two significant changes were detected comparing the FTIR spectra of the unaged and aged S-CNF films. The high-intensity O=S=O peak present in the unaged film decreased to a shoulder of much smaller intensity in the aged film, while the C–O–S absorption peak was not observed in the aged film and, instead, a new broad peak was now visible at considerably higher wavenumber (shifting from 805 to 877 cm^{-1}). These spectral changes, particularly those related with the C–O–S vibration, are an indication that significant desulfation occurred during aging, i.e., hydrolysis of sulfate ester groups covalently bound to the cellulose backbone and subsequent formation of free sulfate species. A similar degradation pathway has been reported for phosphorylated CNF films subjected to moist-heat aging, where hydrolysis of phosphate groups attached to cellulose was also observed [14]. The release and accumulation of free sulfate species (namely HSO_4^-) within the S-CNF films further acidified the films during aging, thereby intensifying the cellulose degradation via acid-catalyzed hydrolysis. In contrast, such significant modifications were not observed in the $NaBH_4$-treated films, for which the FTIR spectra of the unaged and aged S-CNF$_{NaBH4}$ films were similar, as clearly shown in Fig. 7; the only relevant difference was a small decrease in the relative intensity of the C–O–S peak after aging (808 cm^{-1} peak versus most intense peak at 985 cm^{-1}). Even if partial hydrolysis of the sulfate groups occurred in the S-CNF$_{NaBH4}$ films, the accumulation of free sulfate species did not lead to pH reduction (as shown in Fig. 2b) due to the buffering effect of the $B(OH)_4^-/B(OH)_3$ conjugated pair formed during $NaBH_4$ hydrolysis. In sum, $NaBH_4$ treatment mitigated aging-induced chemical modifications, resulting in much greater chemical stability of the S-CNF$_{NaBH4}$ films compared with the untreated films.

Additionally, the surface chemistry of the unaged and aged films was evaluated by XPS, with the most relevant results summarized in Table 2.

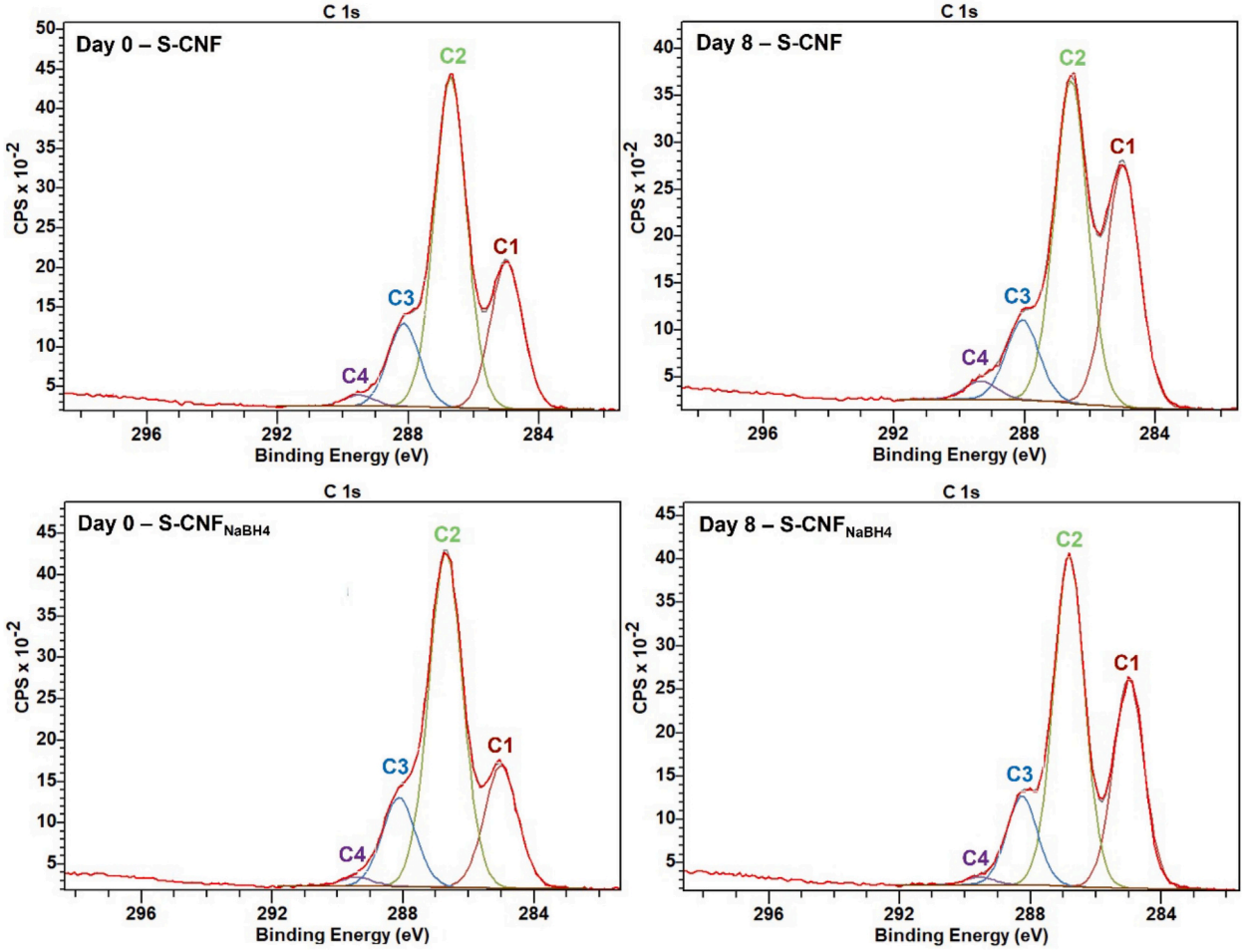

Fig. 8. High-resolution XP spectra with peak fitting in the region of carbon binding energies for the S-CNF and S-CNF$_{NaBH4}$ films before aging and after eight days of aging.

The high-resolution XP spectra with peak-fitting in the region of carbon binding energies are also shown in Fig. 8.

The presence of C (50–55 atm%), O (37–43 atm%), S (1.8–3.1 atm%) and N (0.8–3.4 atm%) was confirmed in the survey spectra of all films based on the observation of the C 1 s, O 1 s, S 2p and N 1 s signals. Additionally, the Na 2 s peak (about 4%) was identified in the $NaBH_4$-treated films. About 1% of boron (B 1 s peak) was also observed in the XP spectrum of the unaged S-CNF_{NaBH4} film; however, this signal was not detectable at the surface of the corresponding aged film, probably due to migration of the borate species from the outermost surface to the bulk during aging. It is interesting to note that the N content (and the N/C ratio) decreased from the neat CNF films to $NaBH_4$-treated films (N/C ratio changing from 0.06 to 0.07 to 0.01–0.02), indicating loss of this element at the surface of the films, regardless of aging. This could be probably related to ammonia volatilization when the medium is buffered at pH ca. 9, supporting the results of FTIR spectroscopy for the S-CNF_{NaBH4} films (NH_4^+ conversion to volatile NH_3). From the calculated S/C ratios (Table 2), it is also possible to observe that before aging both film types (with and without added $NaBH_4$) presented the same S/C ratio of 0.06. Nevertheless, after eight days of aging, the S/C ratio of the neat S-CNF film was reduced to half the value, whereas that of the S-CNF_{NaBH4} film remained unchanged. Together with the FTIR results, this confirms that the incorporation of $NaBH_4$ prior to film formation mitigated chemical changes associated with sulfate groups during aging. On the other hand, the O/C ratio decreased with aging for both S-CNF and S-CNF_{NaBH4} films, from 0.86 to 0.71 and from 0.81 to 0.67, respectively, indicating a reduction in the relative oxygen content at the surface of the aged films.

As shown in Fig. 8, all films showed four main components after peak-fitting of the high-resolution C 1 s spectra: aliphatic carbon (C1: C–H, C–C, C=C); carbon in C–O bonds (C2), which was the dominant contribution; carbon associated with the O–C–O or C=O bonds (C3); and carbon in O–C=O bonds (C4), as the less prominent contribution. Among these components, C1 exhibited the most significant variation with aging, increasing in both S-CNF and S-CNF_{NaBH4} films. Inversely, the C2 and C3 components decreased in both film types after aging. Regarding the C4 component, assigned to O–C=O bonds, a slight increase from about 2 to 3% was observed for the aging of the neat S-CNF film, indicating the formation of oxidized carbon species during moist-heat aging. A similar trend was reported by Zhang et al. [36] for thermally aged cellulose nanocrystal films (containing sulfate groups).

The decrease with aging of atomic oxygen content relative to atomic carbon content and the increase of the C1 component relative to C2 component can be related to the prevalence of acid-catalyzed dehydration reactions over acid-catalyzed cellulose hydrolysis. For the neat S-CNF films, these reactions can occur simultaneously during aging due to the acidic conditions of the medium. While hydrolysis of the cellulose chains increases oxygen content (introduction of OH groups), dehydration reactions (e.g., alkenes and ketones formation with H_2O removal) decrease oxygen content and C2 component and increase C1 component. The final oxygen and carbon contents and the relative proportion of C1s components will be affected by the overall balance of these reactions.

Table 2
XPS atomic ratios (O/C, S/C and N/C) and results of the peak fitting of C 1 s signal for the S-CNF and S-CNF_{NaBH4} films before aging and after eight days of aging.

	Atomic ratios			C 1 s components (%)*			
Film	O/C	S/C	N/C	C1	C2	C3	C4
Day 0 – S-CNF	0.86	0.06	0.07	25.9	57.6	14.5	2.0
Day 8 – S-CNF	0.71	0.03	0.06	36.6	48.6	12.1	2.8
Day 0 – S-CNF_{NaBH4}	0.81	0.06	0.02	22.1	60.3	16.0	1.7
Day 8 – S-CNF_{NaBH4}	0.67	0.06	0.01	32.8	52.0	14.0	1.2

* C 1 s components are normalized to 100%. C1 is attributed to carbon linked only to hydrogen or to carbon (–C–H; –C–C, C=C), C2 corresponds to carbon linked to a single oxygen (–C–O), C3 is assigned to O–C–O or –C=O bonds, and C4 is due to O–C=O bonds [35].

3.6. *Effect of moist-heat aging on the thermal properties of the S-CNF and S-CNF_{NaBH4} films*

The thermal behavior of the S-CNF and S-CNF_{NaBH4} films before and after eight days of aging was evaluated by thermogravimetric analysis. The results are expressed in Table 3, and the resulting thermograms and the corresponding derivative curves are shown in Fig. 9.

As shown in Table 3 and Fig. 9, $NaBH_4$ treatment significantly altered the thermal degradation profile of the S-CNF films, affecting the onset degradation temperature (T_{on}), temperature(s) of maximum degradation rate (T_{max}) and char residue amount. Prior to aging, the $NaBH_4$-treated film exhibited better thermal stability, as evidenced by the higher T_{on} and T_{max} values compared with those of the untreated film. In detail, the unaged S-CNF_{NaBH4} film displayed a T_{on} of 253 °C and a T_{max} of 256 °C (single degradation peak between 150 and 300 °C), while the unaged S-CNF film showed a lower T_{on} (194 °C) and two degradation peaks at lower temperatures (T_{max} of 198 and 249 °C). The char residue at 1000 °C obtained for the S-CNF_{NaBH4} film was also slightly higher than that of the neat S-CNF film. The presence of sulfate functional groups in cellulose materials is known to reduce T_{on} and T_{max} [37]. This phenomenon is attributed to the formation of sulfuric acid during heat degradation of the films, which catalyzes dehydration reactions [38]. Therefore, residual borate species present in the S-CNF_{NaBH4} film may have partially mitigated this acid-catalyzed degradation pathway, resulting in higher T_{on} and T_{max} values compared with the neat S-CNF film. Furthermore, the higher cellulose DP of the unaged S-CNF_{NaBH4} film (801 versus 569) likely also contributed to its enhanced thermal stability, as longer cellulose chains generally require higher energy for thermal degradation.

After eight days of aging, the S-CNF_{NaBH4} film continued to exhibit higher thermal stability. In fact, the aged S-CNF_{NaBH4} film displayed T_{on} and T_{max} values close to those of the unaged film, showing that the thermal stability was not changed under the aging conditions used. On the other hand, owing to the pronounced depolymerization experienced by the S-CNF films during aging, the T_{on} of the aged film decreased compared with the unaged homologue. Overall, the $NaBH_4$ treatment introduced borate species that provided higher thermal stability to the S-CNF_{NaBH4} films before and after aging compared with the corresponding untreated S-CNF films.

In summary, the improved stability against aging of the S-CNF_{NaBH4} films compared to that of the neat S-CNF films, was primarily attributed to the combined alkalizing and buffering effects of the boron-containing species formed through $NaBH_4$ hydrolysis. It should be noted that alkalinization alone, for instance, by adjusting the pH to ca. 9 with NaOH, did not provide the same level of chemical stabilization as that obtained by $NaBH_4$ addition: the resulting film exhibited a tensile strength of 31 MPa, a Young's modulus of 4.2 GPa and a color difference (ΔE) of 6.4 after eight days of aging, corresponding to visually

Table 3
Thermogravimetric data of the S-CNF and S-CNF_{NaBH4} films before aging and after eight days of aging.

Film	T_{on} (°C)*	T_{max} (°C)	Char residue (%)**
Day 0 – S-CNF	194	198/249	28.8
Day 8 – S-CNF	183	210/245	32.8
Day 0 – S-CNF_{NaBH4}	253	256	31.4
Day 8 – S-CNF_{NaBH4}	251	253	23.7

* The T_{on} was determined graphically from the thermograms of each film as the intersection point of two tangents drawn near the first degradation step.

** The char residue was calculated as the ratio between the final mass at 1000 °C and the mass at 150 °C (dry basis).

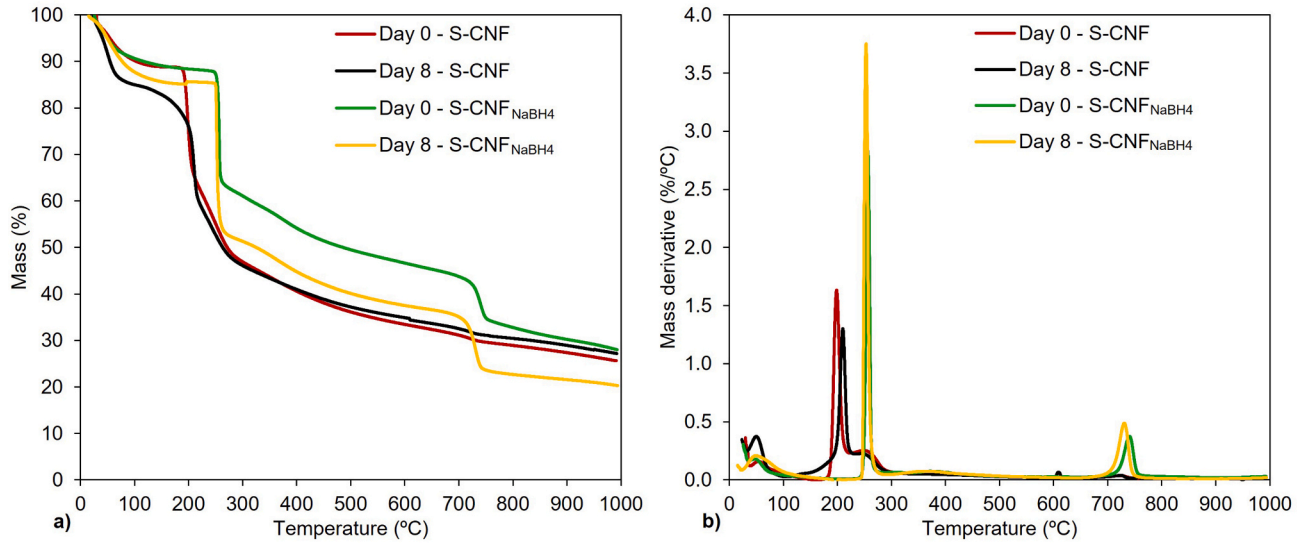

Fig. 9. Thermograms (a) and derivative curves (b) of the S-CNF and S-CNF$_{NaBH4}$ films before aging and after eight days of aging.

perceptible yellowing. These are worse results than those obtained with the $NaBH_4$ treatment, showing the advantage of the new approach proposed in this work.

4. Conclusions

This work demonstrates that sulfated CNF films are extremely vulnerable to moist-heat aging. After only two days at 80 °C and 65% RH, there was a sharp reduction in the cellulose DP, evidencing extensive acid-catalyzed hydrolysis of the cellulose chains. Additionally, pronounced modifications in pH, crystallinity, morphology, and thermal stability of the films occurred with aging, which culminated in severe mechanical deterioration of the films along with significant color changes. The hydrolysis of sulfate ester bonds, leading to the formation of acidic sulfate species, likely contributed to film acidification and accelerated cellulose depolymerization and degradation during aging.

In contrast, the incorporation of $NaBH_4$ prior to film preparation effectively mitigated the detrimental effects of moist-heat aging. The $NaBH_4$ treatment increased, and more importantly, buffered the pH of the S-CNF$_{NaBH4}$ films at around 9 during aging, thereby suppressing cellulose depolymerization, attenuating sulfate ester hydrolysis, and preserving crystallinity and morphology. Consequently, the $NaBH_4$-treated films submitted to the same conditions of moist-heat exposure presented significantly improved mechanical properties and color stability: e.g., after eight-days aging, tensile strength of approximately 40 MPa and Young's modulus of 6 GPa for the aged S-CNF$_{NaBH4}$ film (versus 3 MPa and 0.6 GPa, respectively, for the aged S-CNF film); minimal color changes ($\Delta E = 1.7$) for the aged S-CNF$_{NaBH4}$ film (versus $\Delta E = 39.6$ for the aged S-CNF film). Furthermore, the thermal stability was also improved for the $NaBH_4$-treated films before and after aging.

The stabilization effect imparted by the $NaBH_4$ treatment can be attributed mostly to the buffering effect of borates/boric acid formed during the self-hydrolysis of $NaBH_4$. This acid/base pair can neutralize acidic species formed during film aging (like H_2SO_4 and HSO_4^-), limiting the acid-catalyzed reactions related to cleavage of cellulosic glycosidic bonds and chromophore generation.

Overall, these findings clearly indicate that the addition of an appropriate amount of $NaBH_4$ is an effective chemical stabilization strategy for enhancing the resistance of highly sulfated CNF films to moist-heat aging, expanding their potential for long-term applications by preserving key functional properties under hygrothermal stress.

CRediT authorship contribution statement

Ricardo Almeida: Writing – review & editing, Writing – original draft, Methodology, Investigation, Conceptualization. **Ana Ramos:** Writing – review & editing, Methodology, Investigation. **Verner Håkonsen:** Writing – review & editing, Methodology, Investigation. **Jonas Deuermeier:** Methodology, Investigation. **Thaddeus Maloney:** Writing – review & editing, Supervision. **Naceur Belgacem:** Writing – review & editing, Supervision. **José Gamelas:** Writing – review & editing, Writing – original draft, Supervision, Project administration, Methodology, Funding acquisition, Conceptualization.

Funding

The present research was supported by the R&D Project "BIO-BASED2UC - Exploring novel bio-based materials and their applications in conservation and restoration with a new interdisciplinary team" (Project number: 101186492) funded by the European Research Executive agency - European Commission, and by the PhD grant of Ricardo O. Almeida (2022.11471.BD; https://doi.org/10.54499/2022.11471.BD), funded by the Fundação para a Ciência e Tecnologia (FCT). The authors are also very grateful for the support granted by the Research Unit of Fiber Materials and Environmental Technologies (FibEnTech-UBI), through the Projects with references UID/00195/2025 (https://doi.org/10.54499/UID/00195/2025) and UID/PRR/00195/2025 (https://doi.org/10.54499/UID/PRR/00195/2025), funded by the FCT, IP/MECI. The Research Council of Norway is also acknowledged for the support to the Norwegian Micro- and NanoFabrication Facility, NorFab, project number 295864. The authors also acknowledge FCT for the financial support through projects LA/P/0037/2020, UIDP/50025/2020 and UIDB/50025/2020 of the Associate Laboratory Institute of Nanostructures, Nanomodelling and Nanofabrication – i3N.

Declaration of competing interest

The authors declare that they have no known competing financial interests or personal relationships that could have appeared to influence the work reported in this paper.

Data availability

Data will be made available on request.

References

[1] S.R.D. Petroudy, B. Chabot, E. Loranger, M. Naebe, J. Shojaeiarani, S. Gharehkhani, B. Ahvazi, J. Hu, S. Thomas, Recent advances in cellulose nanofibers preparation through energy-efficient approaches: a review, Energies 14 (2021) 6792, https://doi.org/10.3390/en14206792.

[2] D. Pradhan, A.K. Jaiswal, S. Jaiswal, Emerging technologies for the production of nanocellulose from lignocellulosic biomass, Carbohydr. Polym. 285 (2022) 119258, https://doi.org/10.1016/j.carbpol.2022.119258.

[3] K. Dhali, M. Ghasemlou, F. Daver, P. Cass, B. Adhikari, A review of nanocellulose as a new material towards environmental sustainability, Sci. Total Environ. 775 (2021) 145871, https://doi.org/10.1016/j.scitotenv.2021.145871.

[4] R.O. Almeida, T.C. Maloney, J.A.F. Gamelas, Production of functionalized nanocelluloses from different sources using deep eutectic solvents and their applications, Ind. Crop. Prod. 199 (2023) 116583, https://doi.org/10.1016/j.indcrop.2023.116583.

[5] Y. Wang, H. Liu, X. Ji, Q. Wang, Z. Tian, P. Fatehi, Production of nanocellulose using acidic deep eutectic solvents based on choline chloride and carboxylic acids: a review, Int. J. Biol. Macromol. 245 (2023) 125227, https://doi.org/10.1016/j.ijbiomac.2023.125227.

[6] S. Wang, L. Zhang, K.A. Khan, M.W. Ullah, Y. Fan, Z. Wang, Deep eutectic solvents as a 'multifunctional operating platform' for nanocellulose production and modification: a review on sustainable composite advancements, Mater. Sci. Eng. R. Rep. 165 (2025) 101025, https://doi.org/10.1016/j.mser.2025.101025.

[7] R. Montenegro, E. Rincón, A. Rodríguez, Z. González, Manufacturing sulfated cellulose nanofibers using a unique combined DES-based pretreatment-functionalization protocol for metal ion decontamination through porous adsorbents, Carbohydr. Polym. 349 (2025) 122974, https://doi.org/10.1016/j.carbpol.2024.122974.

[8] J.A. Sirviö, J. Ukkola, H. Liimatainen, Direct sulfation of cellulose fibers using a reactive deep eutectic solvent to produce highly charged cellulose nanofibers, Cellulose 26 (2019) 2303–2316, https://doi.org/10.1007/s10570-019-02257-8.

[9] R. Almeida, A. Ramos, V. Håkonsen, T. Maloney, J. Gamelas, Functionalized cellulose nanofiber films as potential substitutes for Japanese paper, Carbohydr. Polym. Technol. Appl. 8 (2024) 100573, https://doi.org/10.1016/j.carpta.2024.100573.

[10] R.O. Almeida, E. Ferraz, A. Ramos, V. Håkonsen, M.L. Puertas, J.A.F. Gamelas, High-optical-performance composite films of deep eutectic solvent pretreated-cellulose nanofibrils and fibrous clay minerals, Biomacromolecules 26 (2025) 6430–6443, https://doi.org/10.1021/acs.biomac.5c00376.

[11] M. Jaouahar, E.-H. Ablouh, Z. Hanani, B. Jaklič, M. Spreitzer, F.-Z. Semlali, A. Ait Benhamou, Y. Samih, M. El Achaby, H. Sehaqui, Preparation and characterization of sulfated nanocellulose: from hydrogels to highly transparent films, Int. J. Biol. Macromol. 260 (2024) 129464, https://doi.org/10.1016/j.ijbiomac.2024.129464.

[12] R. Almeida, A. Ramos, V. Håkonsen, T. Maloney, N. Belgacem, J. Gamelas, Moist-heat aging of phosphorylated cellulose nanofibril films: influence of phosphorus content and residual lignin, Polym. Degrad. Stab. 245 (2026) 111866, https://doi.org/10.1016/j.polymdegradstab.2025.111866.

[13] C.H.M. Camargos, G. Poggi, D. Chelazzi, P. Baglioni, C.A. Rezende, Strategies to mitigate the synergistic effects of moist-heat aging on TEMPO-oxidized nanocellulose, Polym. Degrad. Stab. 200 (2022) 109943, https://doi.org/10.1016/j.polymdegradstab.2022.109943.

[14] A. Sakiyama, T. Saito, A. Moores, M. Kato, S. Fujisawa, Aging of phosphorylated cellulose nanofibers under moist-heat conditions, Biomacromolecules 27 (2026) 451–458, https://doi.org/10.1021/acs.biomac.5c01635.

[15] M. Henriksson, L.A. Berglund, P. Isaksson, T. Lindström, T. Nishino, Cellulose nanopaper structures of high toughness, Biomacromolecules 9 (2008) 1579–1585, https://doi.org/10.1021/bm800038n.

[16] L. Segal, J.J. Creely, A.E. Martin, C.M. Conrad, An empirical method for estimating the degree of crystallinity of native cellulose using the X-ray diffractometer, Text. Res. J. 29 (1959) 786–794, https://doi.org/10.1177/004051755902901003.

[17] M.C. Area, H. Cheradame, Paper aging and degradation: recent findings and research methods, BioResources 6 (2011) 5307–5337, https://doi.org/10.15376/biores.6.4.5307-5337.

[18] R. Grzeschik, D. Schäfer, T. Holtum, S. Küpper, A. Hoffmann, S. Schlücker, On the overlooked critical role of the pH value on the kinetics of the 4-nitrophenol NaBH4-reduction catalyzed by noble-metal nanoparticles (Pt, Pd, and Au), J. Phys. Chem. C 124 (2020) 2939–2944, https://doi.org/10.1021/acs.jpcc.9b07114.

[19] R. Retnamma, A.Q. Novais, C.M. Rangel, Kinetics of hydrolysis of sodium borohydride for hydrogen production in fuel cell applications: a review, Int. J. Hydrog. Energy 36 (2011) 9772–9790, https://doi.org/10.1016/j.ijhydene.2011.04.223.

[20] R. Retnamma, A.Q. Novais, C.M. Rangel, L. Yu, M.A. Matthews, Kinetic modeling of self-hydrolysis of aqueous NaBH4 solutions by model-based isoconversional method, Int. J. Hydrog. Energy 39 (2014) 6567–6576, https://doi.org/10.1016/j.ijhydene.2014.02.035.

[21] A. Lopalco, A.A. Lopedota, V. Laquintana, N. Denora, V.J. Stella, Boric acid, a Lewis acid with unique and unusual properties: formulation implications, J. Pharm. Sci. 109 (2020) 2375–2386, https://doi.org/10.1016/j.xphs.2020.04.015.

[22] S. Zervos, I. Alexopoulou, Paper conservation methods: a literature review, Cellulose 22 (2015) 2859–2897, https://doi.org/10.1007/s10570-015-0699-7.

[23] S. Bolan, H. Wijesekara, D. Amarasiri, T. Zhang, P. Ragályi, M. Brdar-Jokanović, M. Rékási, J.-Y. Lin, L.P. Padhye, H. Zhao, L. Wang, J. Rinklebe, H. Wang, K.H. M. Siddique, M.B. Kirkham, N. Bolan, Boron contamination and its risk management in terrestrial and aquatic environmental settings, Sci. Total Environ. 894 (2023) 164744, https://doi.org/10.1016/j.scitotenv.2023.164744.

[24] A.D. French, Idealized powder diffraction patterns for cellulose polymorphs, Cellulose 21 (2014) 885–896, https://doi.org/10.1007/s10570-013-0030-4.

[25] S. Zervos, Natural and accelerated ageing of cellulose and paper: a literature review, in: Cellulose: Structure and Properties, Derivatives and Industrial Uses, Nova Publishing, New York, USA, 2010, pp. 155–203.

[26] S. Zervos, Characterization of changes induced by ageing to the microstructure of pure cellulose paper by use of a gravimetric water vapour adsorption technique, Cellulose 14 (2007) 375–384, https://doi.org/10.1007/s10570-007-9125-0.

[27] S.M. Santos, J.M. Carbajo, E. Quintana, D. Ibarra, N. Gomez, M. Ladero, M. E. Eugenio, J.C. Villar, Characterization of purified bacterial cellulose focused on its use on paper restoration, Carbohydr. Polym. 116 (2015) 173–181, https://doi.org/10.1016/j.carbpol.2014.03.064.

[28] M.T.R. Bhuiyan, N. Hirai, N. Sobue, Changes of crystallinity in wood cellulose by heat treatment under dried and moist conditions, J. Wood Sci. 46 (2000) 431–436, https://doi.org/10.1007/BF00765800.

[29] J. Xia, Z. Zhang, W. Liu, V.C.F. Li, Y. Cao, W. Zhang, Y. Deng, Highly transparent 100% cellulose nanofibril films with extremely high oxygen barriers in high relative humidity, Cellulose 25 (2018) 4057–4066, https://doi.org/10.1007/s10570-018-1843-y.

[30] C. Lin, Q. Deng, Y. Hu, L. Huang, Y. Ni, S. Cao, X. Ma, Effects of hemicellulose content on TEMPO-mediated selective oxidation, and the properties of films prepared from bleached chemical pulp, Cellulose 27 (2020) 1043–1054, https://doi.org/10.1007/s10570-019-02844-9.

[31] W.S. Mokrzycki, M. Tatol, Colour difference ΔE - a survey, Mach. Graph. Vis. 20 (2011) 383–411.

[32] A.W. Smith, Bleaching in paper conservation, Restaurator 33 (2012) 223–248, https://doi.org/10.1515/res-2012-0011.

[33] Ú. Fillat, P. Vergara, J.C. Villar, N. Gómez, Structural properties of coated papers with cellulosic nanofibres using different metering systems and drying technologies, Prog. Org. Coat. 179 (2023) 107543, https://doi.org/10.1016/j.porgcoat.2023.107543.

[34] X. Liu, Y. Xu, H. Jia, Y. Zhao, H. Hou, Y. Zhang, NH3 release during the evaporation of different types of atmospheric precipitation: a case study in Changchun, China, Sci. Rep. 15 (2025) 31117, https://doi.org/10.1038/s41598-025-15872-2.

[35] M.N. Belgacem, G. Czeremuszkin, S. Sapieha, A. Gandini, Surface characterization of cellulose fibres by XPS and inverse gas chromatography, Cellulose 2 (1995) 145–157, https://doi.org/10.1007/BF00813015.

[36] C. Zhang, R. Cha, R. Li, L. Tang, K. Long, Z. Zhang, L. Zhang, X. Jiang, Cellophane or Nanopaper: which is better for the substrates of flexible electronic devices? ACS Sustain. Chem. Eng. 8 (2020) 7774–7784, https://doi.org/10.1021/acssuschemeng.9b06956.

[37] M. Jaouahar, E.-H. Ablouh, Z. Hanani, M. Humar, M.E. Achaby, H. Sehaqui, Comprehensive characterization of hygroscopic, fire-retardant and thermally insulating sulfated nanocellulose aerogel, Chem. Eng. J. 506 (2025) 160236, https://doi.org/10.1016/j.cej.2025.160236.

[38] P. Li, J.A. Sirviö, S. Hong, A. Ämmälä, H. Liimatainen, Preparation of flame-retardant lignin-containing wood nanofibers using a high-consistency mechano-chemical pretreatment, Chem. Eng. J. 375 (2019) 122050, https://doi.org/10.1016/j.cej.2019.122050.